AE:221 Aerodynamics

Assignment 1: Airfoil Analysis using Xfoil / Xflr5

Sambhav Jain (SC17B038)

(Department of Aerospace Engineering)
Indian Institute of Space Science and Technology
(Dated: March 9, 2019)

The characteristics of the airfoil using Xflr5 is studied in this assignment. The values of the drag, lift and moment coefficients are studied for the Airfoils- ClarkV, rg15 and fx74cl5140. The trends were observed with the changing reynolds number for these airfoils. Variation for various NACA airfoils were also observed for the changing maximum thickness, maximum camber and the position of maximum camber .

I. INTRODUCTION

XFLR5 is an analysis tool for airfoils, wings and planes operating at low Reynolds Numbers. It includes:

XFoil's Direct and Inverse analysis capabilities; Wing design and analysis capabilities based on the Lifiting Line Theory, on the Vortex Lattice Method, and on a 3D Panel Method. It is an interactive program for the design and analysis of subsonic isolated airfoils. Given the coordinates specifying the shape of a 2D airfoil, Reynolds and Mach numbers, XFOIL can calculate the pressure distribution on the airfoil and hence lift and drag characteristics.

The analysis for the airfoils is done using Xflr5 software. The conditions taken for analysis of the airfoil are given below:

S.No.	Parameter	Value
1	Max. iterations	100
2	Number of panels	~ 100
3	Mach	0.000
4	NCrit	9.00
5	Flap hinge X position	0.8c
6	Flap hinge Y position	0.5t

Any section of the wing cut by the plane parallel to the freestream velocity is called an *airfoil*. The airfoil section is same at any spanwise location along the infinite wing, the properties of the airfoil and the infinite wing are identical. Hence, the airfoil data obtained from the analysis are frequently called *infinite wing data*.

To solve the problems, direct analysis of the Xflr5 was used. Each time an XFoil direct analysis is performed and the convergence is achieved, an OpPoint is generated and the values of interest are stored in the currently selected polar object. Data is added to the polar, whether the option to store OpPoints has been activated or not. The tabular data was taken from each graph by exporting the values directly from the Xflr5.

II. PROBLEM ONE

To analyse any two airfoils among the ones assigned to each group. Plot the airfoils, above mentioned graphs and the table. Each airfoil must be analysed for Reynolds numbers, Re = 100,000 to Re = 500,000 with increments of 100,000.

The airfoil taken for the analysis for the problem one are: CLARK V and RG15. The airfoil shapes are given below:

RG-15 8.9%
Thickness = 8.92%
Max. Thick.pos. = 31.00%
Max. Camber = 1.76%
Max. Camber pos. = 40.00%
Number of Panels = 62

FIG. 1. RG15 airfoil shape

CLARK V AIRFOIL
Thickness = 11.64%
Max. Thick.pos. = 30.00%
Max. Camber = 3.42%
Max. Camber pos. = 50.00%
Number of Panels = 33

FIG. 2. CLARK V airfoil shape

The trends for the variation in the various coefficients are given in the following sections where the variation with the Reynolds number from 100,000 to 500,000 in the steps of 100,000 are taken.

II.1. Cl VS Angle of Attack

Although, the individual values of C_l in both the airfoils are different, but the variation trend with the reynolds number is similar in both the airfoils.

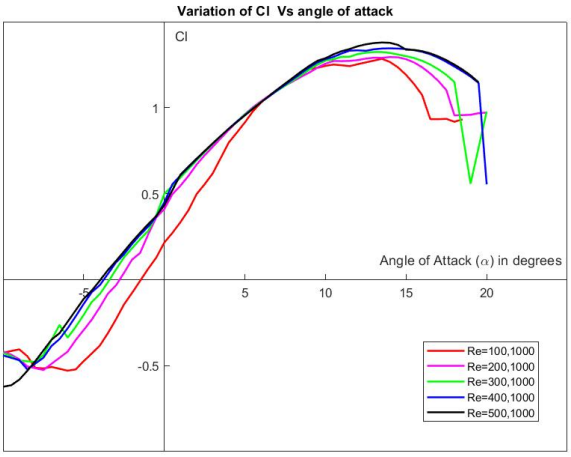

FIG. 3. Variation for the CLARK V airfoil

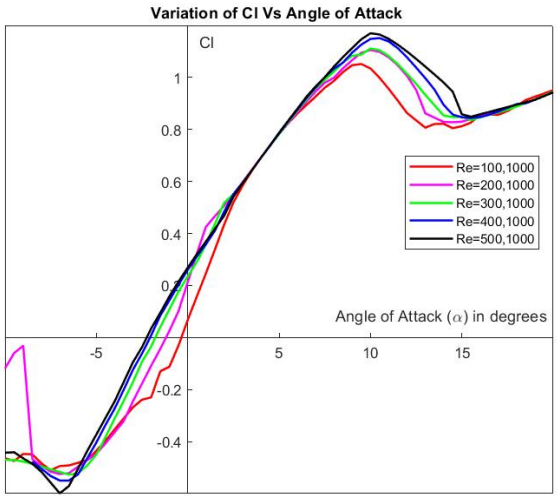

FIG. 4. Variation for the RG15 airfoil

The aforementioned trends in C_l v/s α with increasing reynolds number were observed and are reasoned with as follows

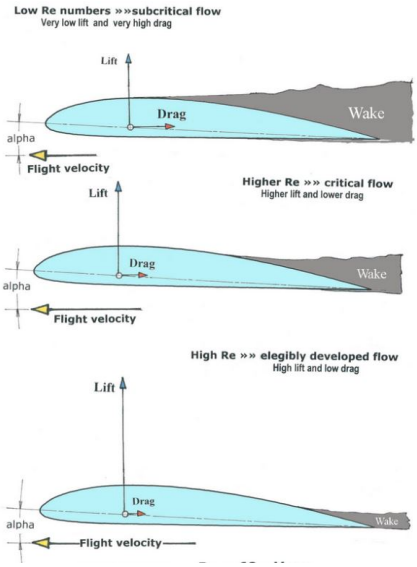

FIG. 5. The figure shows that the wake region decreases with the increase in the flow velocity. The flow incoming sees the wake region as body itself (as it can't enter inside), leading to the lower effective camber of the airfoil. Since, the wake region in turbulent flow is less, the net effective decrease in the camber will be less than that of laminar flow.

1. Horizontal shift in α_{stall} value
   The observed shift in the value of α_{stall} can be reasoned with the delay in the flow separation. As the reynolds number increases, the flow becomes more energised resulting in the delay in separation. Thus, the airfoil now, can bend even further before it encounters the stall.

2. Upward shift of the plots
   As the flow separates a part of the airfoil becomes unreachable for the flow due to the eddies developed. Thus, there exists an apparent change in the airfoil structure as seen by the flow. As the flow separation decreases with an increase in the reynolds number, there is an apparent increase in the camber due to changes in the mean camber line which can be understood from figure 1. As the per the classical thin airfoil theory, the value of the lift coefficient is :
   $C_l = 2\pi \times [\alpha + \frac{1}{\pi}\int \frac{dz}{dx}(cos\theta_o - 1)\, d\theta_o]$
   As per the above explanation, we found that the stall angle is increasing with the reynolds number, the Cl_{max} value will increase as it is directly proportional to angle of attack.

It is observed experimentally that as we go from the transition region to the turbulent region, the value of Cl_l increases and just as it enters the turbulent region, the value of the coefficient doesn't alter much.

II.2. Cd VS Angle of Attack

The trends in the variation of the C_d value with the reynolds number is similar in both the airfoils and can be seen from the following graphs:

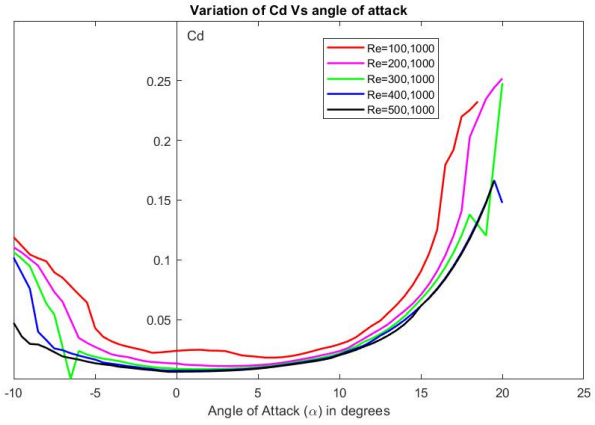

FIG. 6. Variation for the CLARK V airfoil

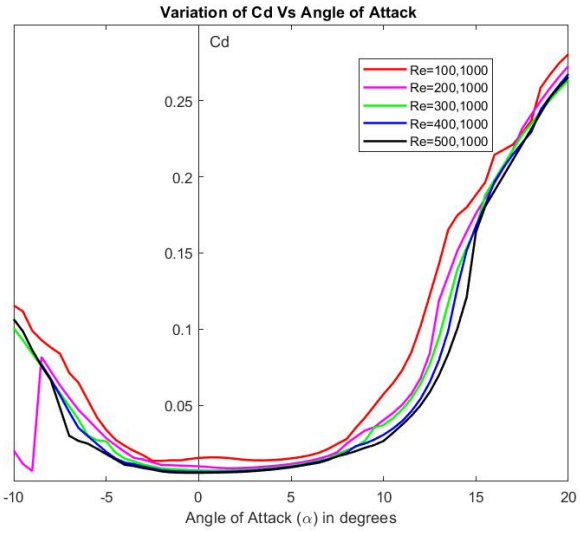

FIG. 7. Variation for the RG15 airfoil

The aforementioned variations in the value of C_d with an increase in the value of reynolds number is reasoned as follows Total drag for an airfoil consists of both the skin friction drag and the pressure drag. Airfoil being a slender object, the contribution of both skin friction drag and pressure drag is significant. With increase in reynolds number, the separation wake is decreased for a particular α and hence the pressure drag decreases. On the other hand there is also an increase in the skin friction drag value as the profile becomes steeper. But, it was observed experimentally that the increase in latter if lesser than the decrease in the former hence resulting in a decrease in the total drag and drag coefficient.

Moreover, the term in the denominator of the formula of C_d given by,

$C_d = \frac{DragForce}{\frac{1}{2}\rho u^2}$

, has velocity sqaured term, which will effectively decrease the drag coefficient on increasing reynolds number.

II.3. Cl/Cd VS Angle of Attack

The variation in the Cl/Cd ratio is also similar for both the airfoils with the change in the reynolds number.

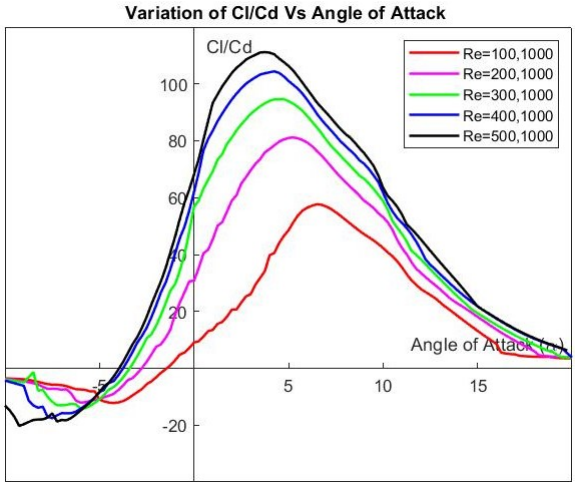

FIG. 8. Variation for the CLARK V airfoil

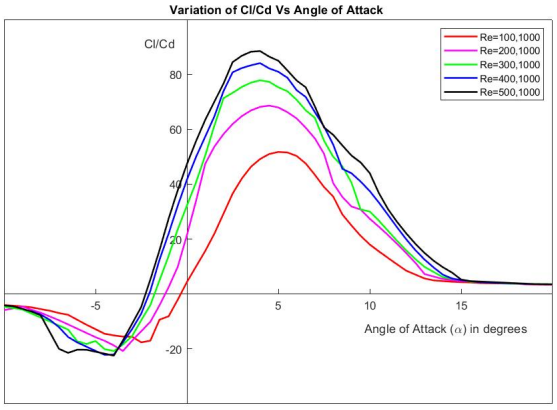

FIG. 9. Variation for the RG15 airfoil

The variations mentioned in the above plot of C_l/C_d vs α are reasoned as follows :
Since there was an increase in C_l value and a decrease in C_d value for all points in the plot (Figures 3, 4, 5 and 6), the value of C_l/C_d is bound to increase at every point. Further, it is also observed that there is a decrease

in the $\alpha^{C_l/C_d max}$ value with increase in reynolds number. The maximum value of the ratio has a great aerodynamic significance, as it shows the maximum efficiency that an aerofoil can has.

II.4. Cl VS Cd

The variation in the plot is similar for both the airfoils with the change in the reynolds number.

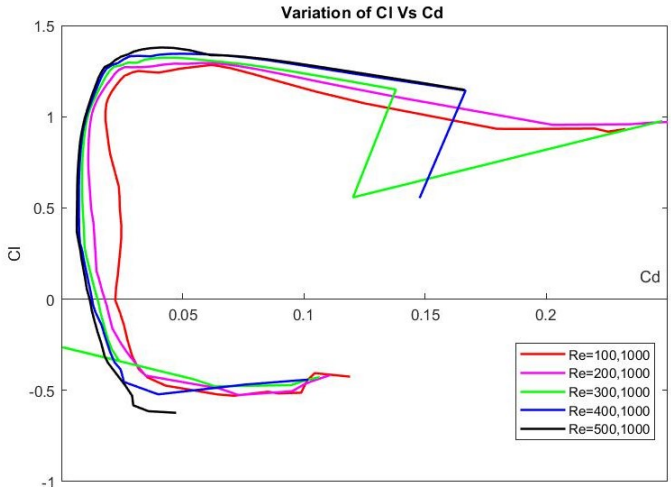

FIG. 10. Variation for the CLARK V airfoil

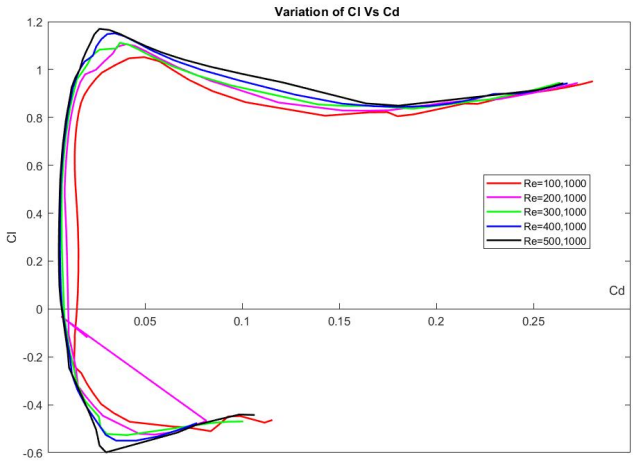

FIG. 11. Variation for the RG15 airfoil

The Cl VS Cd curve gives us the value of $(\frac{C_l}{C_d})_{max}$ by the slope as shown in the below figure:

The value of maximum ratio by the slope measurement shows that the aerodynamic efficiency increases with the reynolds number. This matches with the results of the Cl/Cd Vs angle of attack curves. Hence, the reason for

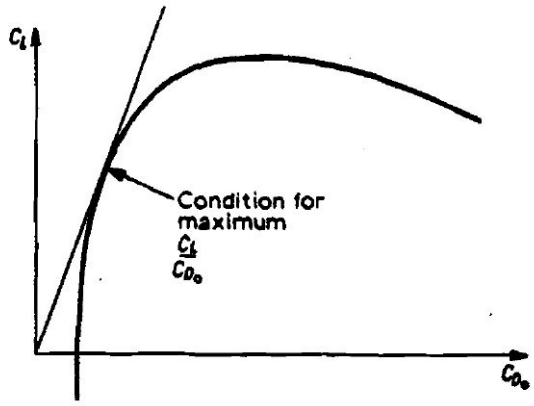

FIG. 12. Maximum value of the Cl/Cd ratio from the Cl VS Cd curve

this variation could be explained same as that of the previous one.

II.5. Cm VS Angle of Attack

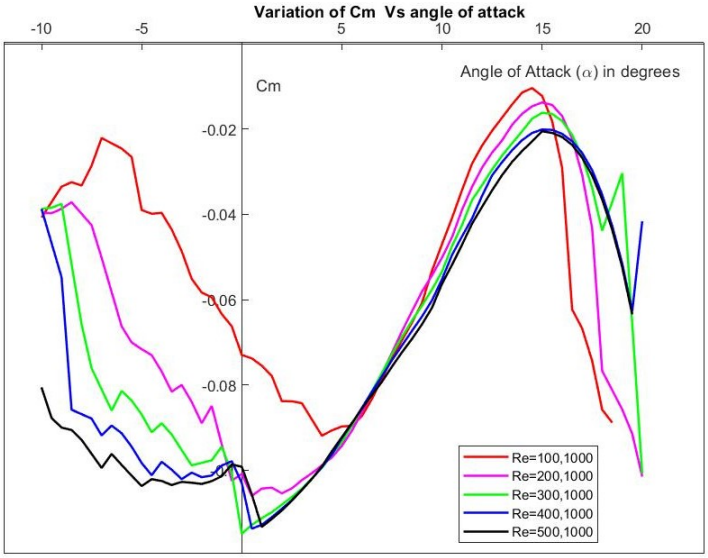

FIG. 13. Variation for the CLARK V airfoil

The Cm is observed to be increasing in the magnitude with the increase in the reynolds number. The concepts from the classical airfoil theory can be utilised to explain this variation. The theory for the cambered airfoil, predicts the value of moment coefficient as:
$Cm_{c/4} = Cm_{ac} - \frac{C_l}{4}$
The camber increases the Cm as its directly proportional to it and can be seen as well after deriving using a particular case. The maxima and the minima corresponds to the LE and TE flow separation. All the above mentioned variations are depicted in the tables placed next.

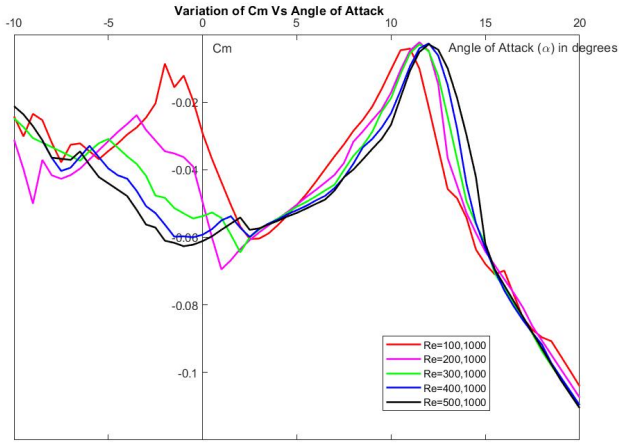

FIG. 14. Variation for the RG15 airfoil

Re	Cl max	alpha stall	alpha 0	Cl/Cd max	Alpha	Cd	Cl
100000	1.283996	13.5	-1.5	57.68692	6.5	0.018555	1.070388
200000	1.290597	13	-2.75	80.98671	5	0.011889	0.962828
300000	1.323478	13	-3.5	94.02278	4	0.009336	0.877776
400000	1.345047	14	-4	104.0918	4	0.008438	0.878325
500000	1.379133	13.5	-4	111.0539	3.5	0.007526	0.835802

FIG. 15. salient features of ClarkV airfoil

Re	Cl/Cd max	alpha	Cl	Cd	Cl max	alpha max	alpha=0
100000	51.74181	5	0.781733	0.015108	1.051603	9.5	-0.25
200000	68.59519	4.5	0.73743	0.01075	1.105668	10	-1.25
300000	77.83653	4	0.690285	0.008868	1.111234	10	-1.75
400000	84.08189	4	0.690407	0.008211	1.151221	10.5	-2
500000	88.48596	4	0.690906	0.007808	1.169908	10	-2.25

FIG. 16. salient features of RG15 airfoil

III. PROBLEM TWO

Analyse any one of the airfoils among the ones assigned to each group for the effect of trailing edge flaps. Deflection angles to be analysed and compared with are $\delta = -15^o$, 0^o, 15^o and 30^o for Re = 300,000

The airfoil under consideration for the current question is the RG15.(fig. 17)

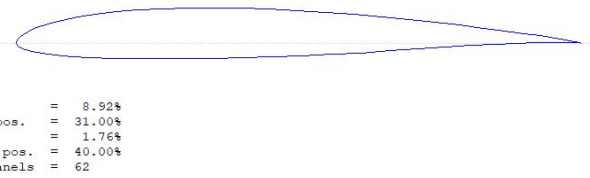

FIG. 17. RG15 airfoil plot with details

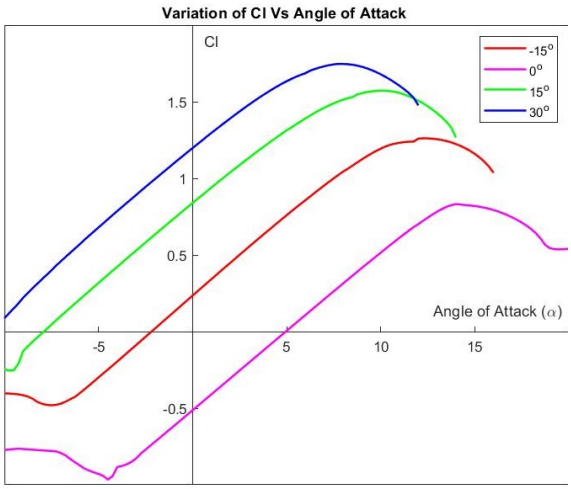

III.1. C_l vs α

The variation in the C_l value is seen to be increasing with the increase in the deflection angle. This variation can be explained in two ways:

1. As the deflection angle is increased, the effective camber is increased. The net increase in the camber of the airfoil leads to the increase in the value of lift.
2. From the classical thin airfoil theory for the cambered airfoils, gives the value of δC_l to be as:
   $\delta C_l = [(\pi - \theta_h) + sin\theta_h)]\eta$
   Here, the η is the deflection angle and θ_h is the coordinate of the hinge position, which is an obtuse angle in our case. As the change in the lift coefficient is directly proportional to the defection angle, it increases with the increase in the angle.

III.2. C_d vs α

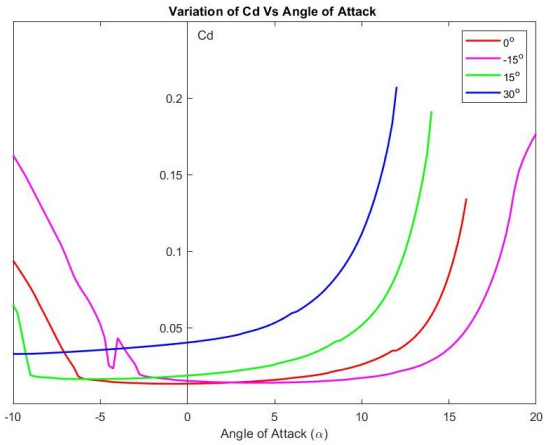

The variation observed for the value of drag coefficient

is that with the increase in the deflection angle, the drag coefficient increases. This could also be attributed to the change in the camber with the deflection angle. As the camber increases, the region for the flow over the upper surface of the airfoil increases. This increase in the flow region makes the flow seperation earlier, hence increasing the drag. This drag value increase will be in case of skin friction drag also, as with the increase in the flow region, the gradients for the velocity increases. The overall increase in the drag can be attributed to the integrated effect of increase in the values of pressure and skin friction drag.

III.3. C_l/C_d vs α

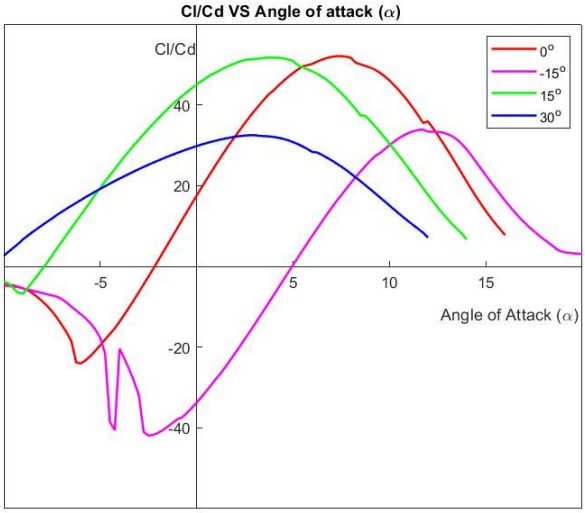

The variation in the Cl/Cd maximum value could be seen to be increasing with the flap deviation angle. As with the increase in the camber with the deviation angle, the value of the Cl value increases greater than that of the Cd, the net ration increases. But the offtrend is shown by deviation angle of 30^o because at high deviation angle of this much value makes the flow to seperate ,much earlier making large increase in the Cd value as compared to the Cl value, thereby, making the net ratio to decrease. This signifies a great significance of deviation angle on the aerodynamic efficiency of the airfoil.

III.4. C_l vs C_d

Taking the maximum slope of the plot shows the similar trend of Cl/Cd max. with the deviation angle, hence, the reason for this would be same as that of the previous plot.

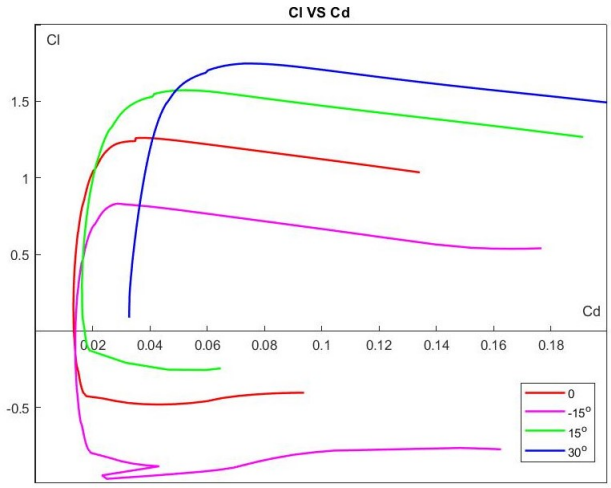

III.5. C_m vs α

In this case, it is observed that with the increase in the deviation angle, the Cm value becomes more negative. This can be explained with the help of classical thin airfoil theory for the thin cambered airfoils, as the Cm given by:
$\delta C_m = [0.5 \times sin\theta_h(cos\theta_h - 1)]\eta$
Here, as the θ_h is an obtuse angle, the net value of δC_m will be negative. And with the increase in defection angle it increases, making the net Cm value to increase more negatively.

Finally the change in the value of angle of attack at zero lift can be again explained by the classical theory as:
$\delta\alpha_{L=0} = -[(\pi - \theta_h) + sin\theta_h]\eta/\pi$
As, the θ_h is an obtuse angle, the net value is negative, showing that angle of attack for the zero lift decreases with the increase on the deviation angle, which satisfies the trend shown by the values.

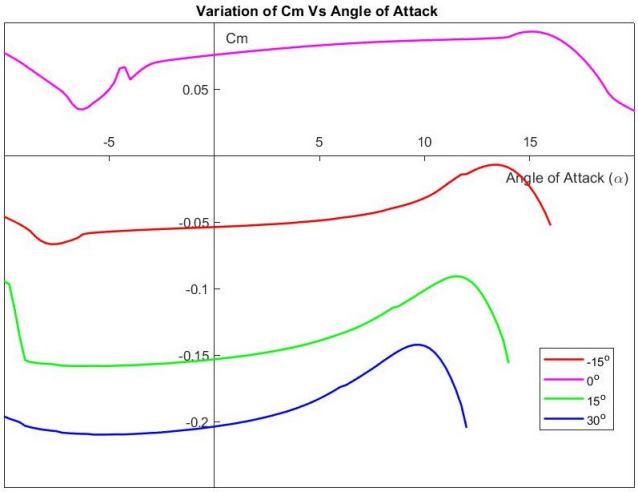

δ	$C_{l,max}$	α_{stall}	$(C_l/C_d)_{max}$	α	C_l	C_d	$\alpha_{L=0}$
-15	0.831815	14	33.87792	11.75	0.681412	0.020114	5
0	1.260834	12.25	52.07214	7.5	0.999795	0.0192	-2
15	1.572207	10	51.73382	4	1.225981	0.023698	-8
30	1.746735	7.75	32.49619	3	1.481094	0.045577	

FIG. 18. salient features of RG15 airfoil with changes in deflection angle

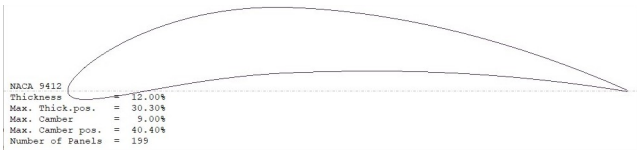

FIG. 23. NACA 9412 airfoil shape

IV. PROBLEM THREE

Study the effect variation of following geometric properties of NACA series airfoils at Re = 300,000.

IV.1. Variation in max camber for NACA x412 series (x=0, 2, 4, 6, 9)

FIG. 19. NACA 0412 airfoil shape

FIG. 20. NACA 2412 airfoil shape

FIG. 21. NACA 4412 airfoil shape

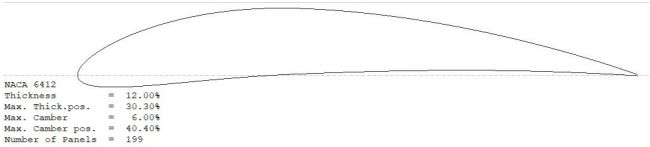

FIG. 22. NACA 6412 airfoil shape

Airfoil	$C_{l,max}$	α_{stall}	$(C_l/C_d)_{max}$	α	C_l	C_d	$\alpha_{L=0}$
NACA0412	1.164754	12.5	53.41021	5.5	0.667839	0.012504	0
NACA2412	1.335056	15	77.15977	6	0.892697	0.011569	-2
NACA4412	1.44348	17.5	91.43501	7	1.202297	0.013149	-4.5
NACA6412	1.649983	11	95.28592	6.5	1.372702	0.014406	-6.5
NACA9412	1.981604	11.5	95.70939	4	1.408901	0.014721	-12.5

FIG. 24. Variation of characteristics with change in max camber of airfoil

IV.1.1. C_l vs α

Stagnation point shift downwards in the airfoil as the camber increases. The stagnation point located at the bottom of an airfoil physically translates to the lift force being acted upon the bottom surface and that's how lift is generated anyway (Newton's 3rd law of motion and not so much as due to the pressure difference above and below the airfoil). min pressure decrease-lift decrease-gradient increase- low alpha stall

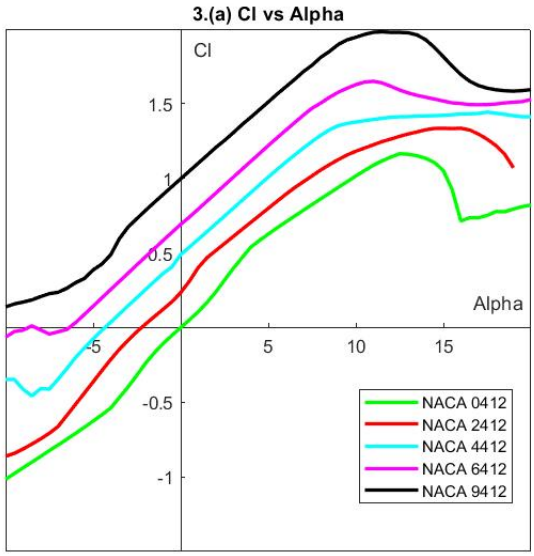

FIG. 25. Variation of C_l vs α with change in max camber

IV.1.2. C_d vs α

An airfoil with higher camber has a higher exposed area for the flow, this implies a higher value of Cd at same angle of attack for a high camber airfoil. Also, for high value of camber, the adverse pressure gradient is higher which implies a higher skin friction drag. more exposed area-more drag-higher adverse pressure gradient- more drag

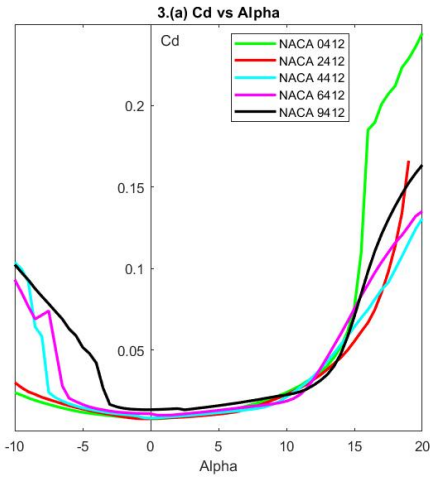

FIG. 26. Variation of C_d vs α with change in max camber

IV.1.3. C_l/C_d vs α

Cl increases more than Cd for change in max camber, therefore Cl/Cd increases for increase in max camber of the airfoil.

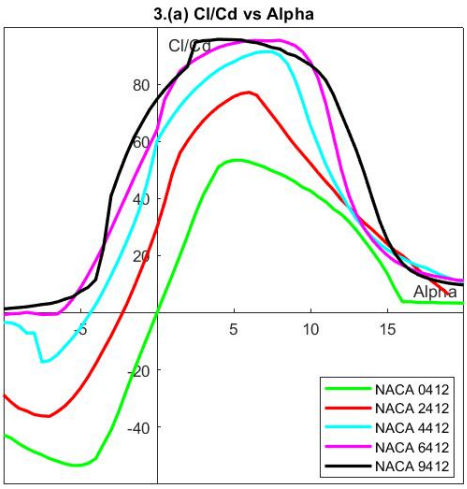

FIG. 27. Variation of C_l/C_d vs α with change in max camber

IV.1.4. C_l vs C_d

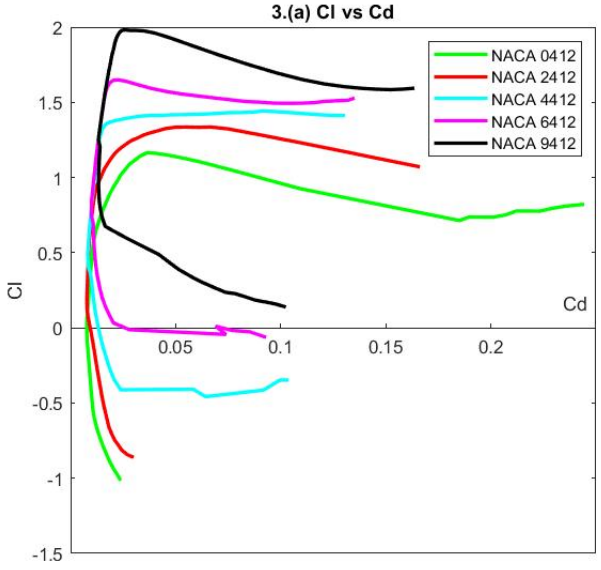

FIG. 28. Variation of C_l vs C_d with change in max camber

The variation of Cl vs Cd moves upwards and rightwards for higher camber, thus following the following relation

$$C_D = C_{D,0} + K(C_L - C_{L,0})^2$$

IV.1.5. C_m vs α

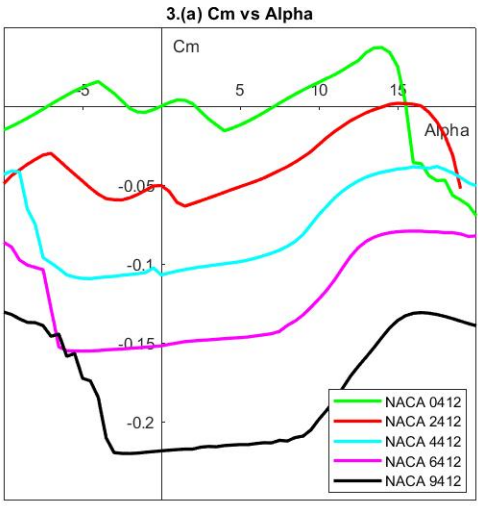

FIG. 29. Variation of C_m vs α with change in max camber

Due to change in max camber, the position of center of pressure doesn't change much therefore Cm is proportional to Cl for not very extreme angle of attack. Therefore, Cm is higher for higher camber airfoil when compared to low camber airfoil.

IV.2. Variation in position of max camber for NACA 4x12 series (x=1, 2, 3, 4, 5)

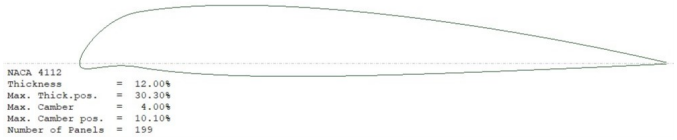

FIG. 30. NACA 4112 airfoil shape

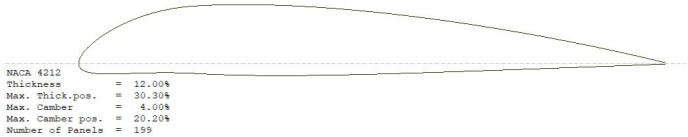

FIG. 31. NACA 4212 airfoil shape

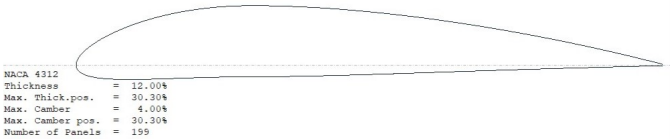

FIG. 32. NACA 4312 airfoil shape

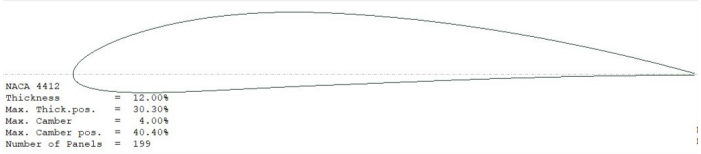

FIG. 33. NACA 4412 airfoil shape

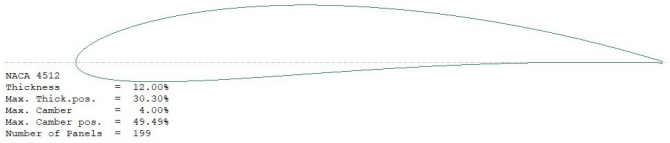

FIG. 34. NACA 4512 airfoil shape

Airfoil	$C_{l,max}$	α_{stall}	$(C_l/C_d)_{max}$	α	C_l	C_d	$\alpha_{L=0}$
NACA4112	1.582997	13.5	51.34746	5	0.889339	0.01732	-4
NACA4212	1.681095	14.5	66.57477	8	1.241017	0.018641	-4
NACA4312	1.496742	11.5	82.67981	9.5	1.404087	0.016982	-4
NACA4412	1.44348	17.5	91.43501	7	1.202297	0.013149	-4.5
NACA4512	1.478366	16.5	99.09368	5	1.045594	0.010552	-4.5

FIG. 35. Variation of characteristics with change in position of max camber of airfoil

IV.2.1. C_l vs α

In case of max camber position being positioned forward, the adverse pressure gradient region increases, i.e. the flow will separate at a smaller angle of attack therefore the stalling angle of attack will be lower.

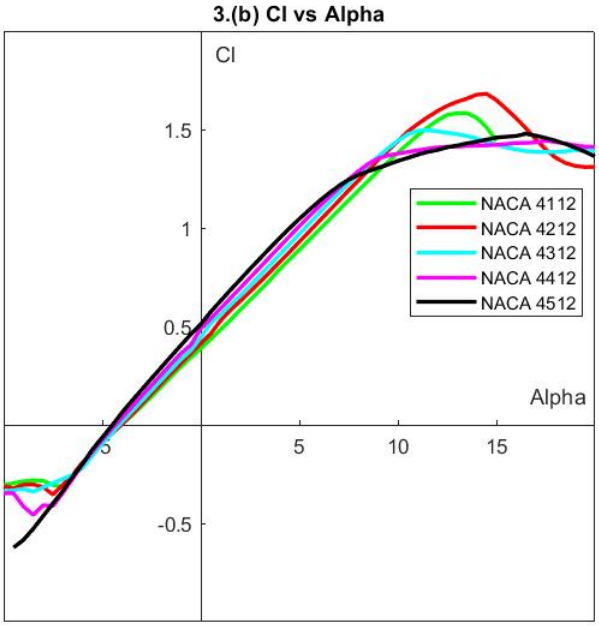

FIG. 36. Variation of C_l vs α with change in position of max camber

IV.2.2. C_d vs α

In case of max camber position being positioned forward, the nose radius increases and thus increasing the pressure drag. Also, the adverse pressure gradient region increases, thereby increasing the turbulent nature of the flow, causing higher skin friction drag.

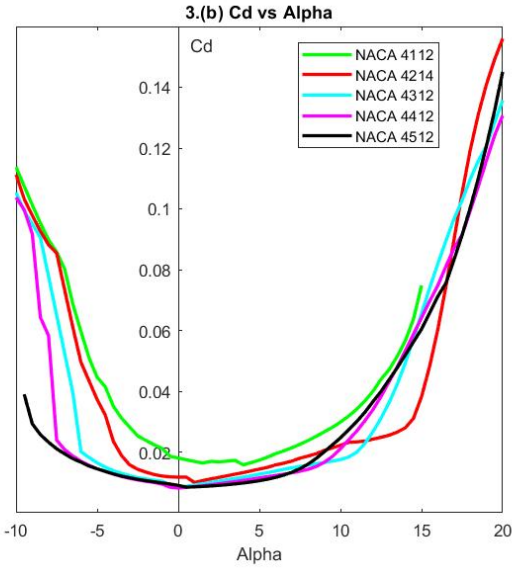

FIG. 37. Variation of C_d vs α with change in position of max camber

IV.2.3. C_l/C_d vs α

The position of maximum Cl/Cd ratio follows the relation
Also, the Cl/Cd ratio for airfoil with forward max camber position is maximum at the lower angle of attack due to early flow separation. $(\frac{C_L}{C_D})_{max} = \sqrt{\frac{\pi \epsilon AR}{C_{D,O}}}$

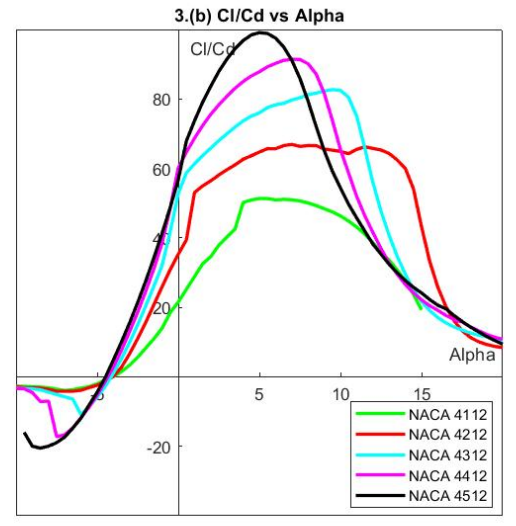

FIG. 38. Variation of C_l/C_d vs α with change in position of max camber

IV.2.4. C_l vs C_d

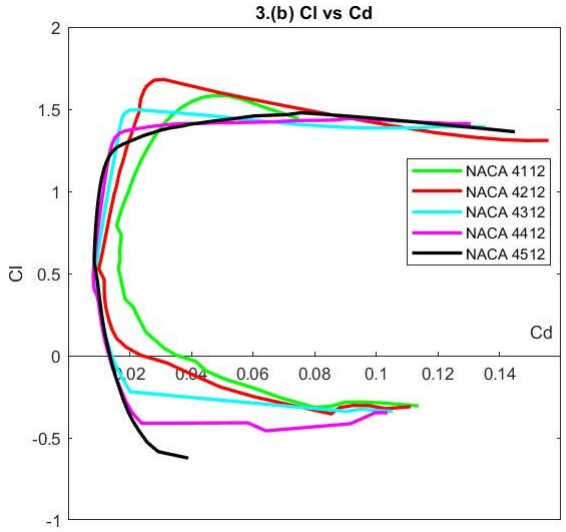

FIG. 39. Variation of C_l vs C_d with change in position of max camber

The variation of Cl vs Cd moves leftwards and lower for airfoil with max camber at a backward position, thus following the following relation
$C_D = C_{D,0} + K(C_L - C_{L,0})^2$

IV.2.5. C_m vs α

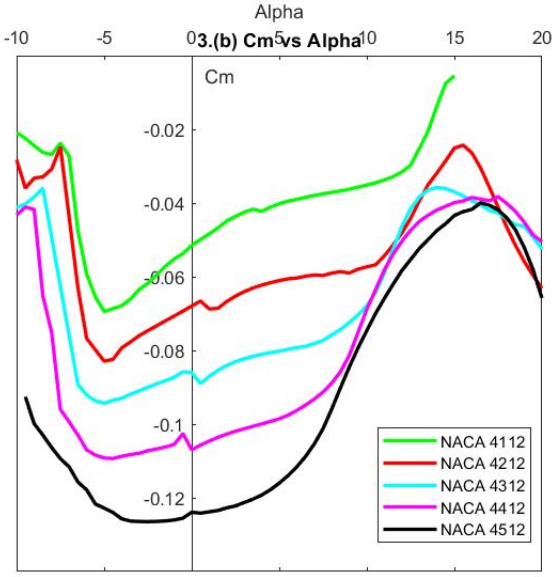

FIG. 40. Variation of C_m vs α with change in position of max camber

Due to change in position of max camber, the position of center of pressure doesn't change much therefore Cm is proportional to Cl for mild angle of attack. Therefore, Cm is lower for forward camber position.

IV.3. Variation in max thickness for NACA 44xx series (xx = 08, 10, 12, 14, 16)

FIG. 41. NACA 4408 airfoil shape

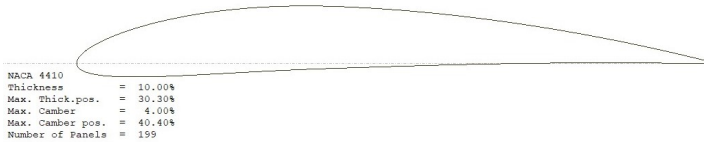

FIG. 42. NACA 4410 airfoil shape

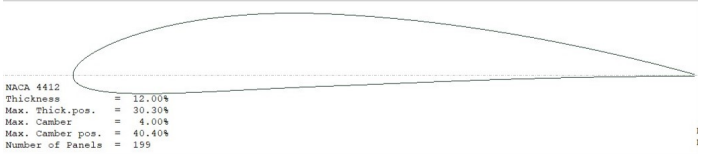

FIG. 43. NACA 4412 airfoil shape

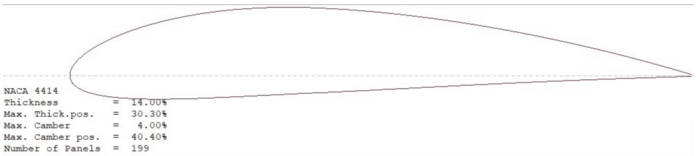

FIG. 44. NACA 4414 airfoil shape

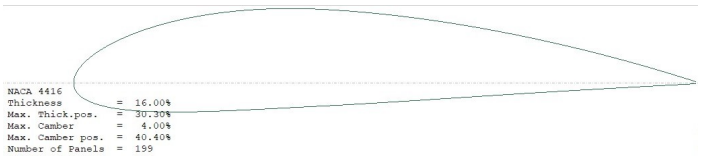

FIG. 45. NACA 4416 airfoil shape

Airfoil	$C_{l,max}$	α_{stall}	$(C_l/C_d)_{max}$	α	C_l	C_d	$\alpha_{L=0}$
NACA4408	1.382213	11	96.50602	5	0.997434	0.010335	-4
NACA4410	1.429706	15.5	94.33492	6.5	1.151115	0.012202	-4
NACA4412	1.44348	17.5	91.43501	7	1.202297	0.013149	-4.5
NACA4414	1.463107	12.5	87.63894	7.5	1.24674	0.014226	-4.5
NACA4416	1.509894	13.5	83.32555	8	1.282608	0.015393	-4.5

FIG. 46. Variation of characteristics with change in max thickness of airfoil

IV.3.1. C_l vs α

For thin airfoils, flow separation position is more sensitive to the angle of attack and therefore the loss of lift is more sudden than thicker airfoils. Also, thicker airfoils have higher Cl_{max} because of lower value of Cp_{min} at stalling angle of attack.

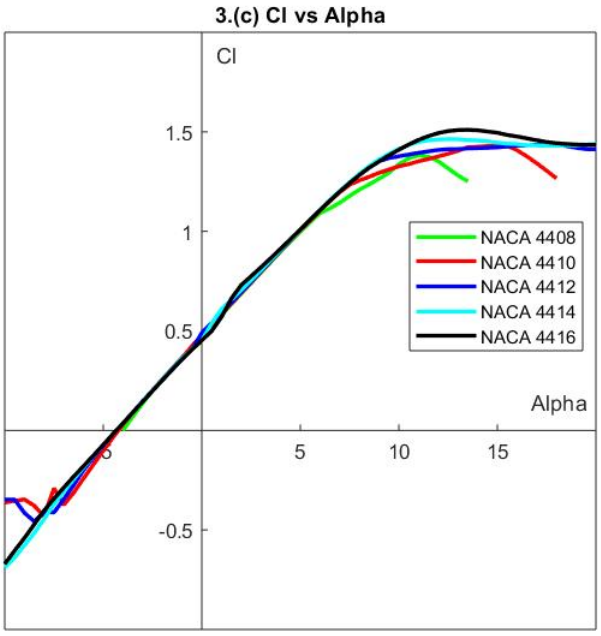

FIG. 47. Variation of C_l vs α with change in max thickness

IV.3.2. C_d vs α

Thicker airfoils have a higher drag because of higher surface area exposed to the flow and higher nose radius. Also, the adverse pressure gradient is higher, therefore the pressure drag is high.

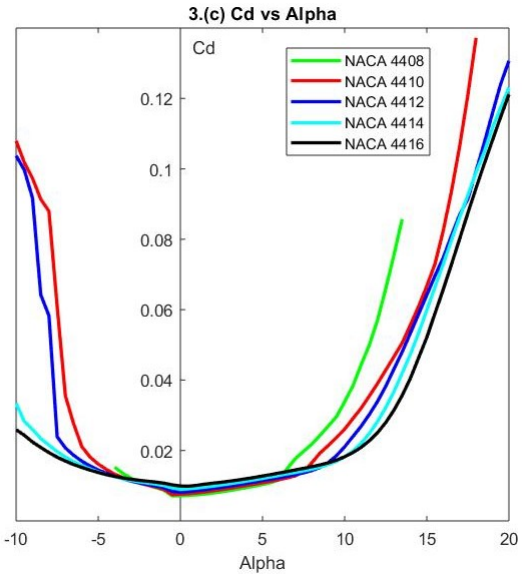

FIG. 48. Variation of C_d vs α with change in max thickness

IV.3.3. C_l/C_d vs α

The position of maximum Cl/Cd ratio follows the relation:
$(\frac{C_L}{C_D})_{max} = \sqrt{\frac{\pi \epsilon AR}{C_{D,O}}}$

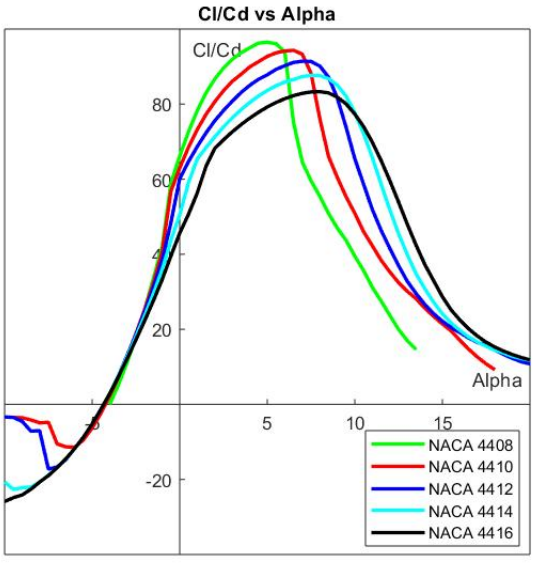

FIG. 49. Variation of C_l/C_d vs α with change in max thickness

The Cd increases steeply at lower angle of attack for thin airfoils therefore Cl/Cd decreases before for such thin airfoils.

IV.3.4. C_l vs C_d

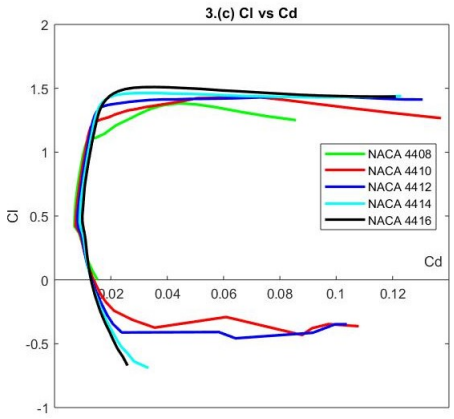

FIG. 50. Variation of C_l vs C_d with change in max thickness

The variation of Cl vs Cd moves upwards and rightwards for higher thickness, thus following the below relation
$C_D = C_{D,0} + K(C_L - C_{L,0})^2$

IV.3.5. C_m vs α

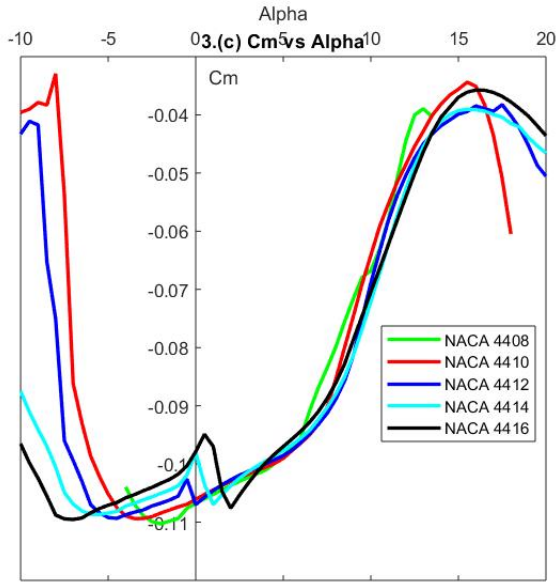

FIG. 51. Variation of C_m vs α with change in max thickness

Due to change in thickness, the position of center of pressure doesn't change much therefore Cm follows the trend of Cl for mild angle of attack. Therefore, Cm is lower for higher thickness.
Generally, the more an airfoil is cambered towards its rear

end, the higher its pitch moment coefficient will be. This is called "rear loading" and is used in order to combine decent thickness with good lift in transsonic airfoils.

V. FX74C15140 ANALYSIS

This analysis prerequisite pertains to the FX74c15140 airfoil which was excluded from analysis in problem one. The following plots were obtained from xflr5. The table is used for the salient features of FX74c15140 airfoil. Both the table and the graphs are included in the APPENDIX.

Appendix

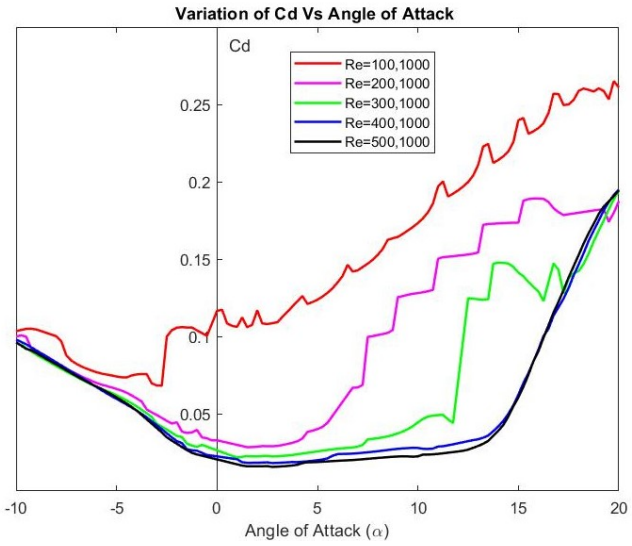

Figure 1: Variations in FX74c15140 airfoil

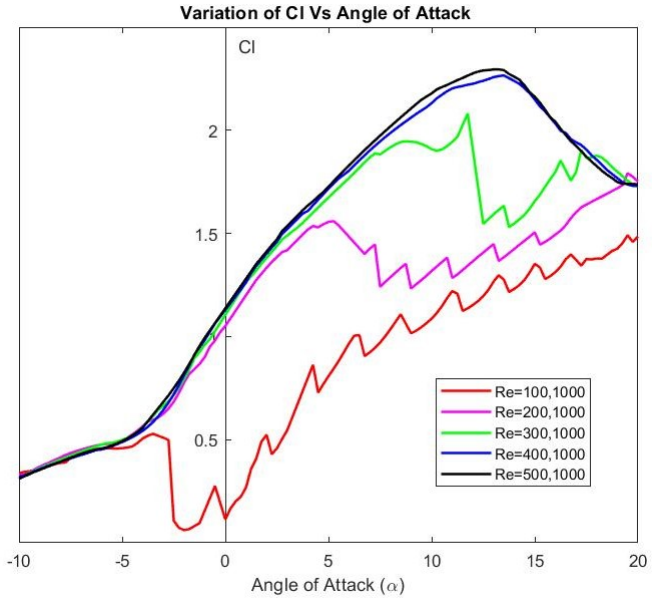

Figure 2: Variations in FX74c15140 airfoil

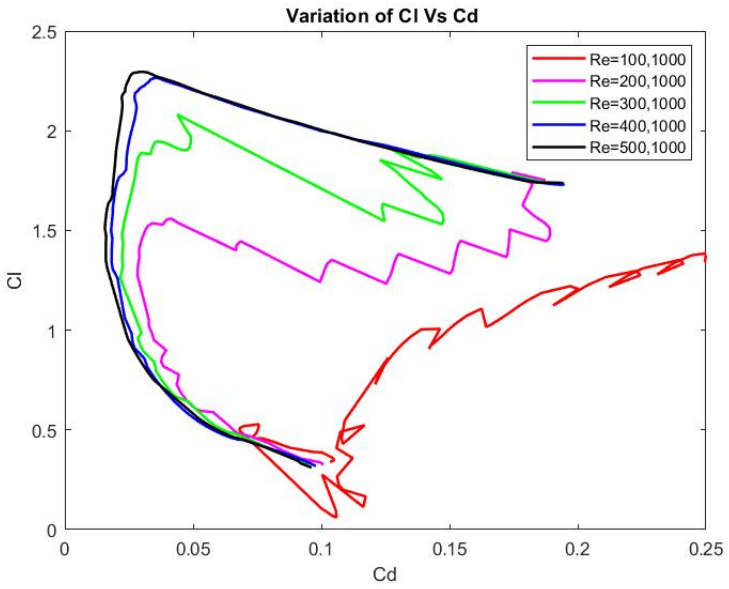

Figure 3: Variations in FX74c15140 airfoil

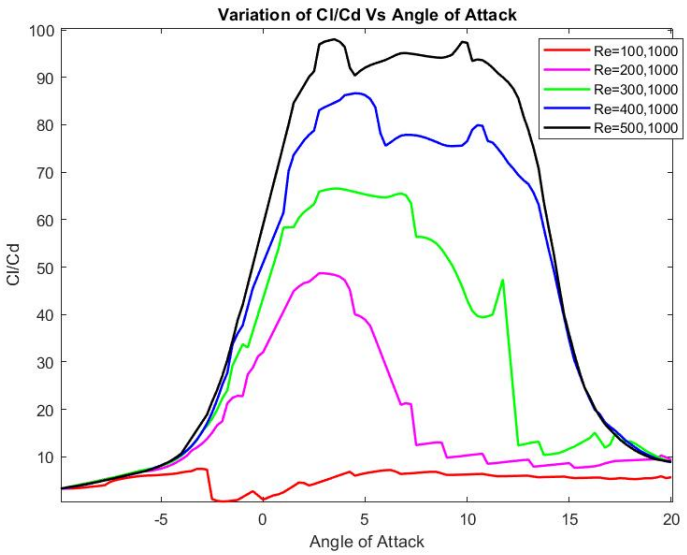

Figure 4: Variations in FX74c15140 airfoil

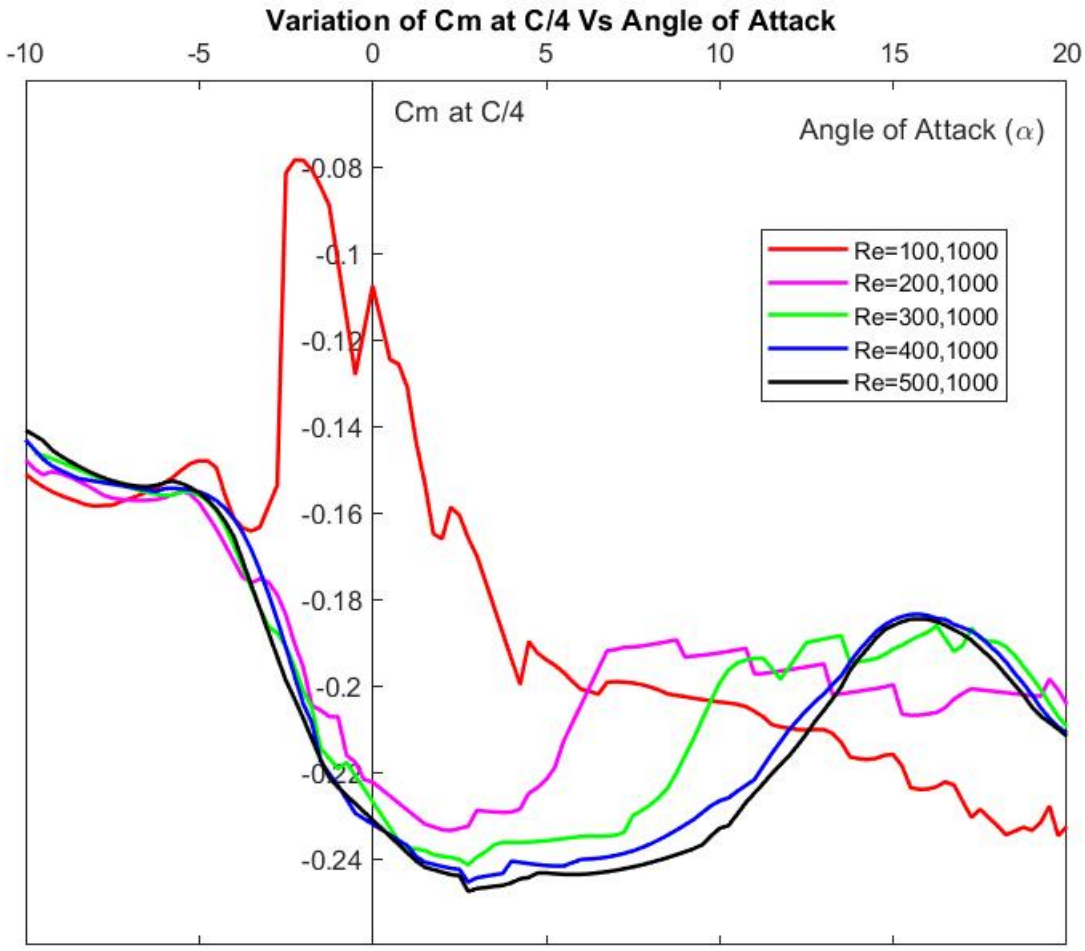

Figure 5: Variations in FX74c15140 airfoil

Re	Cl/Cd	Alpha	Cl	Cd	Cl max	Alpha stall	Alpha=0
100000	9.231163	-2.5	0.569864	0.061733	1.516409	20	-1
200000	50.86653	3	1.469501	0.028889	1.833862	8.5	-14.5
300000	4326.446	0.5	1.08873	0.000252	2.265309	12.5	-15
400000	7823.848	0.5	1.109048	0.000142	2.305397	13	NOT COVE
500000	7935.009	0.5	1.115782	0.000141	2.321378	13	-16

Figure 6: salient features of FX74c15140 airfoil